Journal of Electroanalytical Chemistry 895 (2021) 115440

Contents lists available at ScienceDirect

Journal of Electroanalytical Chemistry

journal homepage: www.elsevier.com/locate/jelechem

# On the activity and stability of $Sb_2O_3$/Sb nanoparticles for the electroreduction of $CO_2$ toward formate

Beatriz Ávila-Bolívar, Vicente Montiel, José Solla-Gullón *

*Institute of Electrochemistry, University of Alicante, Apdo. 99, E-03080 Alicante, Spain*

ARTICLE INFO

*Keywords:*
Activity
$CO_2$ reduction
Electrocatalysis
Formate
$Sb_2O_3$/Sb electrodes
Stability

ABSTRACT

The development of new electrocatalysts with improved properties for the electrochemical reduction of $CO_2$ is being the objective of innumerable contributions. In this contribution, the electrochemical reduction of $CO_2$ to formate on novel carbon-supported antimony nanoparticles (Sb/C NPs) is studied. The carbon-supported $Sb_2O_3$/Sb nanoparticles were synthesised using a simple methodology at room temperature and characterized by transmission electron microscopy, X-ray photoelectron spectroscopy, and X-ray diffraction. The $Sb_2O_3$/Sb/C electrodes were prepared by air-brushed onto a carbon paper and were characterized by scanning electron microscopy and energy-dispersive X-ray spectroscopy. The $Sb_2O_3$/Sb/C electrodes were also electrochemically characterized by cyclic voltammetry and displayed a clear activity for $CO_2$ electroreduction. To evaluate the properties of the electrodes for the reduction of $CO_2$, electrolyses at different potentials were systematically conducted. Hydrogen and formate were the only products found. The faradic efficiency towards formate was found to be about 20%. This FE was in good agreement with previous finding obtained with comparable system. Interestingly, 24-hour tests were carried out to analyse the stability of the material under working conditions. The results indicate that $Sb_2O_3$/Sb-based electrodes display a remarkably better stability than other nanostructured electrocatalysts such as Sn or Bi.

## 1. Introduction

The excessive consumption of fossil fuels has caused a continuous increase of $CO_2$ in the atmosphere, resulting in the adverse effect of climate change and the aggravation of the energy crisis [1–3]. The global warming has encouraged an interest to develop carbon capture, storage and reuse technologies using renewable sources [4–11]. At this respect, the conversion of $CO_2$ into valuable carbonaceous compounds has appealed significant consideration and, among the different approaches capable of transforming $CO_2$, the electrochemical reduction of $CO_2$ is a proven good alternative. Electrochemical $CO_2$ reduction reactions ($ECO_2RR$) are typically carried out under ambient conditions and, additionally, the energy required can be derived from renewable energy sources such as solar and wind, which promotes its viability for large-scale implementation [12–17].

However, it is well-known that $ECO_2RR$ occur at a similar potential range on which the hydrogen evolution reaction (HER) also takes place. Consequently, as reported extensively, $ECO_2RR$ is inevitably accompanied by HER and also displays a complex reaction mechanism with multiple electron transfer processes with manifold coupled consecutives intermediates [18–24]. This scenario gives rise to low activity and poor selectivity toward the desired products which makes the process economically inefficient. In addition, stability issues still need to be significantly improved. For all these reasons, finding more active, selective, energy efficient and durable electrocatalysts represents a major challenge for $ECO_2RR$. At this respect, it is worth noting that a large number of parameters affect the properties of the electrocatalysts including the chemical nature [25–28], atomic composition [29–35], and particle size [36–39], among others. Consequently, several electrocatalysts as well as other experimental conditions such as temperature and pressure [19], pH [40–42], and electrolyte composition [19,20,43–45] have been evaluated for $ECO_2RR$.

Based on the product selectivity, transition and post-transition metals, including mono/bimetallic materials or metal oxides, are grouped taken into consideration the main product of the reaction. In this regard, the main products are carbon monoxide (CO), methane ($CH_4$), ethylene ($C_2H_4$), methanol ($CH_3OH$), formate/formic acid ($HCOO^-$/HCOOH), formaldehyde (HCHO) or ethanol ($CH_3CH_2OH$) [25,46]. Among these, the production of formic acid/formate is particularly interesting due to their wide versatility in multiple practical

* Corresponding author.
*E-mail address:* jose.solla@ua.es (J. Solla-Gullón).

https://doi.org/10.1016/j.jelechem.2021.115440
Received 16 February 2021; Received in revised form 7 May 2021; Accepted 31 May 2021
Available online 2 June 2021

applications [47–52]. In addition, the formic acid can be used as hydrogen storage material [53,54].

For the production of formic acid/formate, Tin and Bismuth based electrocatalysts are amongst the best potential candidates due to their high hydrogen overpotentials and high selectivity toward formate in the aqueous electrolytes [55–61]. However, antimony (Sb), despite having a chemical behaviour similar to Sn and Bi, has received much less attention as an electrocatalyst for the formate production. This lack of attention is probably owing to the low catalytic activity initially reported in previous studies [62]. However, in recent years, a few works have demonstrated the potential of Sb as electrocatalysts for $ECO_2RR$. For instance, Jia et al. [63] revealed that Sb atomic sites supported on *N*-doped carbon were active to produce CO. On the other hand, an improved activity was observed on 2D Sb nanosheets which showed the capability to catalyse the electroreduction of $CO_2$ selectively with a faradic efficiency (FE) for formate of about 84% at −1.06 V vs. RHE due to the exposure of a large number of active edge sites [64]. Also, Jiang et al. [65] discovered that an Sb single atom material consisting of Sb–N4 moieties anchored on *N*-doped carbon can produce formate with high efficiency of 94.0% at −0.8 V vs. RHE.

Interestingly, Sb could enhance its low activity being alloyed with a number of metals to improve their properties. Thus for example, Rasul et al. reported an improved formate FE owing to the presence of Sb in a Sn-Pb-Sb alloy [66,67]. Also, Lima et al. [68] studied the activity of SnSb alloy films as electrocatalysts for the $ECO_2RR$ which presented a high faradaic efficiency for formate production of 96.2% at −1.25 V vs RHE. Despite these previous findings, the synthesis of well-defined and highly dispersed Sb nanoparticles and the study of their electrocatalytic properties for $ECO_2RR$ still remain unexplored.

In the present study, an easy and fast procedure for the preparation of carbon-supported Sb nanoparticles under soft experimental conditions is proposed. These Sb nanoparticles will be physicochemical and electrochemically characterised in order to evaluate their activity for $CO_2$ reduction towards formate in an aqueous electrolyte. Finally, an examination of the stability of the Sb-based electrodes is also included.

## 2. Materials and methods

### 2.1. Chemicals and reagents

$SbCl_3$ (99.9%, Alfa Aesar) was used as Sb precursor. *N*,*N*-Dimethylformamide (DMF, 99.8%, Sigma Aldrich), polyvinylpyrrolidone (PVP, K30, Mw ~55.000, Aldrich), and sodium borohydride ($NaBH_4$ 99%, Aldrich) were used as solvent, capping agent and reducing agent, respectively. Vulcan XC-72 carbon powder (CAS No 1333-86-4, sample number GP 3621) was purchased from Cabot Corporation (Boston, MA, USA). $KHCO_3$ (99.7%, Sigma Aldrich), KCl (99.5%, Emsure) and KOH (85%, Panreac, Barcelona, Spain) were used for the catholyte and anolyte solutions. The ion exchange cross-linked resin Nafion (5 wt% in isopropyl/water solution) was purchased from Alfa Aesar (Ward Hill, MA, USA). Cationic ion exchange membrane Nafion 112 was purchased from DuPont, (Wilmington, DE, USA). All other chemicals were purchased from the highest analytical grade available and were used as received without any further purification. All solutions were prepared using MilliQ ultrapure water (18.2 MΩ cm).

### 2.2. Synthesis of antimony electrocatalysts

The methodology used for the synthesis of the Sb nanoparticles is similar to that previously used in our research group with other metals [69–71] and takes place at room temperature and pressure. In brief, $SbCl_3$ and PVP are initially dissolved in DMF under magnetic stirring. Subsequently, solid $NaBH_4$ is aggregated to the mixture and stirred for 30 min alternating magnetic and ultrasound stirring. After the addition of the reducing agent the solution becomes dark, indicating the reduction of $Sb^{3+}$ to $Sb^0$. For the preparation of carbon supported nanoparticles, appropriate amounts of Vulcan XC-72R carbon powder were subsequently added to the mixture and stirred for at least 30 min under magnetic stirring and ultrasound. Samples with a nominal Sb loading of ca. 20 wt% were prepared. To collect and clean the sample, acetone (about 5 times the volume of the solution) was directly added to the solution. After complete precipitation of the sample, the sample was filtered through a nylon membrane filter of 45 mm (Cat No. MNY045047H, chm by CHMLAB GROUP, Barcelona, Spain), and washed with acetone:water (90:10) mixtures. The nanoparticles were finally dried in an oven at 55 °C for 12 h under vacuum conditions.

### 2.3. Preparation of the Sb-based electrodes

For the manufacture of the electrodes, a catalytic ink was firstly prepared containing the Sb samples, Nafion solution (perfluorosulfonic acid - PTFE copolymer 5% w/w solution, Alfa Aesar) as binder at a Sb/C:Nafion mass ratio of 70:30, and diluted to 2 wt% in absolute ethanol (EMSURE®, Merck, Darmstadt, Germany). The mixture was sonicated for 30 min and the ink was directly sprayed by air brushing technique onto a carbon paper (TGPH-90 from QuinTech, Göppingen, Germany) with a geometric surface area of 9 $cm^2$ which is placed on a hot metallic plate at 90 °C to facilitate solvent evaporation. The final Sb/C loadings were 0.75 mg $cm^{-2}$ and 1.50 mg $cm^{-2}$.

### 2.4. Physicochemical characterisation

The morphology and particle size of the nanoparticles were analysed by transmission electron microscopy (TEM) with a JEOL JEM-1400 Plus microscope (JEOL, Akishima, Tokyo, Japan) working at 120 kV. The samples were dispersed onto a Lacey-covered copper grid and allowed to evaporate in air at room temperature. The crystal structure and phase purity of the nanoparticles were confirmed by powder X-ray diffraction (XRD) and the patterns were obtained with a D8 Advance diffractometer (Bruker, Billerica, MA, USA) fitted with a copper tube. The optical setup included a Ni 0.5% CuKβ filter in the secondary beam so that only CuKα radiation illuminated the sample ($CuK\alpha_1$ = 0.154059 nm and $CuK\alpha_2$ = 0.154445 nm). X-ray photoelectron spectroscopy (XPS) experiments were recorded on a K-Alpha spectrometer (Thermo Scientific, Waltham, MA, USA) using AlKα 1486.6 eV radiation, monochromatised by a twin crystal monochromator and yielding a focused X-ray spot with a diameter of 400 mm, at 3 mA × 12 kV. Deconvolution of the XPS spectra was carried out using a Shirley background. The metal (Sb) loading was experimentally analysed by inductively coupled plasma optical emission spectrometry (ICP-OES) (Perkin Elmer, Optima 4300 D). For that, a known amount of the carbon supported Sb nanoparticles was firstly treated in 65% nitric acid to dissolve Sb. The corresponding solution was then diluted using a 2 wt% $HNO_3$ water solution and finally filtered before being analysed. Scanning electron microscopy (SEM, S-3000 N microscope, Hitachi, Krefeld, Germany, working at 20 kV with a Bruker Xflash 3001 X-ray detector for microanalysis) was employed to analyse the morphology of the electrocatalytic layer of the manufactured electrodes.

### 2.5. Electrochemical characterisation

The electrochemical characterisation of the Sb-based electrodes was performed in a three-electrode configuration glass cell in Ar or $CO_2$-saturated 0.45 M $KHCO_3$ (99.7%, Sigma Aldrich) and 0.5 M KCl (99.5%, Emsure) solution using a platinum wire and an AgCl/Ag (3.5 M KCl) as counter and reference electrodes, respectively. Cyclic voltammetry (CV) experiments were performed using a PGSTAT302N system (Metrohm Autolab B. V., Utrecht, Netherlands). All CV measurements were performed at 25 ± 1 °C. Currents were normalised

by the geometric area of the electrodes. For sake of comparison, a Sb rod (antimony rod, 12.7 mm diameter, 99.99% metals basis, Alfa Aesar) was also employed. $CO_2$ electroreduction electrolyses were performed in an H-type electrochemical cell with divided compartments through a cationic ion exchange membrane (Nafion 112). A $CO_2$-saturated 0.45 M $KHCO_3$ and 0.5 M KCl solution ($CO_2$ continuous flux of 200 mL $min^{-1}$) was used as catholyte. The anolyte was a 1.0 M KOH (85%, Panreac, Barcelona, Spain) solution. The Nafion 112 membrane was previously activated in 0.5 M NaOH for 24 h. A nickel mesh immersed in the anolyte acted as counter electrode. An AgCl/Ag (3.5 M KCl) electrode placed in the catholyte was used as reference electrode. The $CO_2$ electroreduction electrolyses were carried out by chronoamperometry measurements at controlled potential between −1.6 V and −1.9 V for 1.5 h and 24 h.

### 2.6. Analytical determinations

The conversion of $CO_2$ to formate was analysed by ionic chromatography (883 Basic IC plus, Metrohm, with conductivity range of 15,000 μScm$^{-1}$). The mobile phase consisted of 1.8 mM $Na_2CO_3$ and 1.7 Mm $NaHCO_3$. A calibration curve was initially carried out from 0 to 10 ppm in 0.0045 M $KHCO_3$ and 0.005 M KCl (corresponding with a 100 times dilution of the catholyte). The gaseous compounds were analysed by gas chromatography (GC, Hewlett Packard HP 5890 Series II) coupled to a thermal conductivity detector (TCD), the temperature of the injection port was 120°, the detector temperature of 250 °C and the oven of 30 °C. The chromatographic column was a MS-13X and a Ar stream was the carrier gas. The gaseous compounds were collected from the sealed cathodic compartment during the electrolyses in a Tedlar Bag (1 Liter) and analysed in the GC-TCD with aliquots of 250 μL by a Hamilton syringe. A previous external calibration was carried out with pure gaseous samples of $O_2$, $N_2$, CO, $H_2$ and $CO_2$.

## 3. Results and discussion

### 3.1. Characterization of the Sb/C nanoparticles

To evaluate the synthesis of Sb nanoparticles, different PVP to $SbCl_3$ stoichiometric ratios and amounts of DMF were initially studied. In the optimized recipe, 0.228 g of $SbCl_3$ were dissolved into 75.84 g of DMF, then, 0.112 g of PVP and 0.116 g of $NaBH_4$ were added under stirring conditions. Fig. S1 shows TEM images of the pure Sb nanoparticles, prepared under these conditions before washing and filtering (in DMF solution). Under these conditions, isolated and small (about 5 nm) $Sb_2O_3$/Sb nanoparticles can be easily observed. However, when samples are washed and filtered with acetone, they tend to agglomerate even in the presence of carbon as supporting material. Fig. 1 displays some representative TEM images of the carbon-supported Sb nanoparticles. The images indicate that the dispersion of the Sb nanoparticles is reasonably good. Fig. S2 also presents one of these images at higher magnification. To estimate the mean diameter of the nanoparticles, about 200 particles from different TEM images were analysed. The corresponding particle size histogram is reported in Fig. S3. The particle size was found to be about 28 ± 11 nm but some clusters, formed by aggregated Sb nanoparticles of about 40–150 nm, were also observed indicating that the dispersion can be still improved. From ICP-OES measurements, the metal loading was found to be about 14.5 wt%, slightly lower than the nominal one (20 wt%) which is attributed to the residual presence of DMF trapped in the porosity of the carbon Vulcan.

Fig. S4 displays the XRD diffractogram of the Sb/C NPs. The XRD profile displays 4 diffraction peaks corresponding to the (222), (400), (440) and (622) crystal planes of a $Sb_2O_3$ cubic phase (senarmontite) [72]. The presence of Sb oxides is expected due to spontaneous oxidation during the exposure to air.

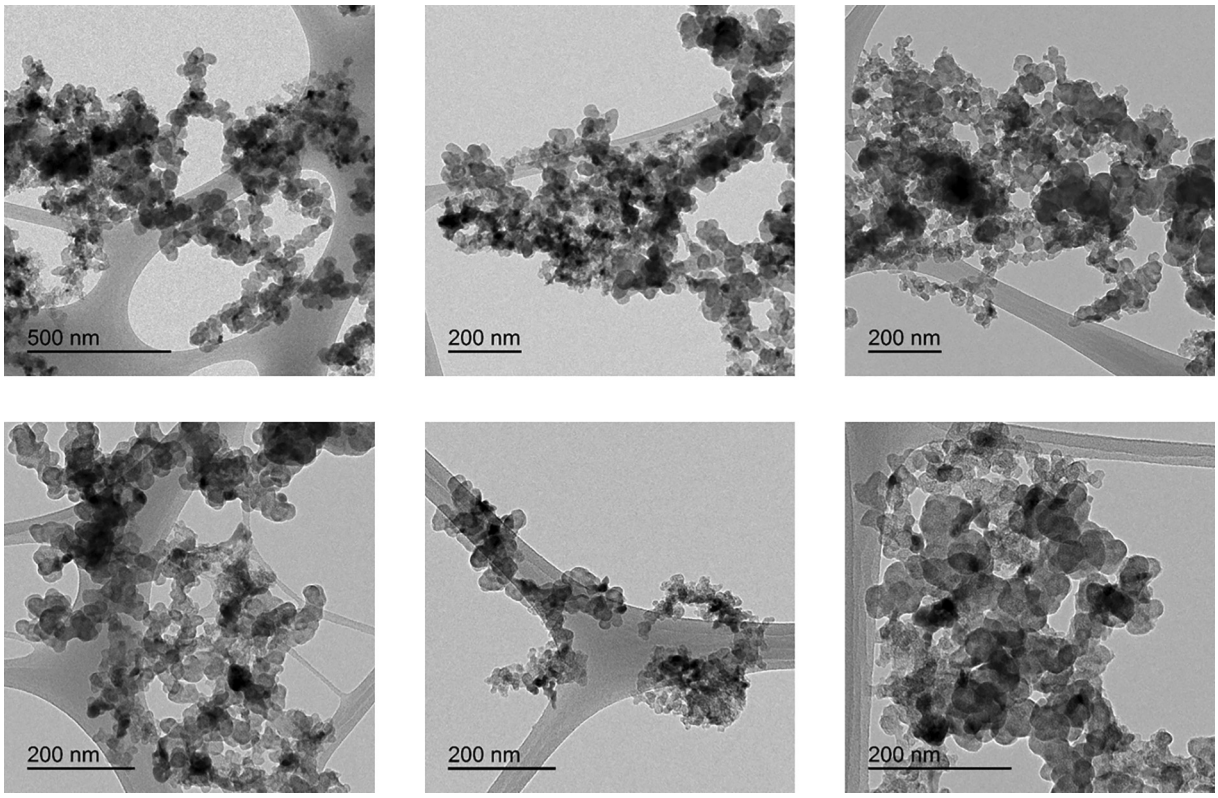


**Fig. 1.** Representative TEM images of the prepared Sb/C nanoparticles.

XPS measurements were also performed to study the surface chemistry of our material. Fig. S5 shows the XPS spectrum of the Sb 3d region. It is worth noting that the Sb 3d5/2 signal overlaps with the O 1s spectrum. As expected any signal attributed to $Sb^0$ is observed and the Sb 3d3/2 signal shows the presence of two binding energy contributions at 540.3 and 542.0 eV which can be related to $Sb^{3+}$ and $Sb^{5+}$, respectively [73–75], thus confirming that the SbNPs present an oxidised character.

### 3.2. Sb/C-Toray paper electrodes characterization

As described in the experimental section, the Sb/C sample was used to manufacture Sb-based electrodes by air-brushed onto a carbon paper. Two electrodes with different catalytic loadings of 0.75 and 1.50 mg SbC $cm^{-2}$ were prepared. The Sb-based electrodes were characterised (surface and cross section) by SEM. Fig. 2 shows some representative SEM images of the electrodes. The images evidence how the Sb/C ink covers homogenously the carbon fibbers leading to a uniform and compact catalytic layer, independently of the metal loading. At higher magnification, some of the Sb clusters previously mentioned can be also observed.

Cross section SEM images of the electrodes show that the thickness of the catalytic layer (CL) increases for increasing metal loading (Fig. S6). Thus, for 0.75 mg Sb/C NPs·$cm^{-2}$, the thickness of the CL is about 17.8 μm, while, for 1.50 mg Sb/C NPs·$cm^{-2}$, is about 36.1 μm.

### 3.3. Electrochemical characterisation

The electrochemical characterisation of the Sb-based electrodes was performed in an Ar and $CO_2$ saturated 0.45 M $KHCO_3$ and 0.5 M KCl solution. For sake of comparison, a Sb rod was also studied under the same conditions. Fig. 3 reports the cyclic voltammograms obtained in Ar and $CO_2$ saturated solutions with the Sb-based electrodes. In Ar saturated solution, an oxidation contribution can be clearly observed (onset potential at about −0.5 V vs AgCl/Ag) associated with the electrochemical oxidation of Sb to $Sb_2O_3$. In the negative going sweep, the reduction of this $Sb_2O_3$ to Sb is observed at about −0.9 V vs AgCl/Ag. A very similar voltammetric behaviour is observed with the Sb rod (Fig. S7). The larger double layer contribution observed in the Sb-based electrodes is due to the presence of the carbon substrates (toray paper and Vulcan XC-72R). In both cases, Sb-based electrodes and Sb rod, the onset potential of the hydrogen evolution reaction (HER) takes places at about −1.5 V vs AgCl/Ag. However, in $CO_2$ saturated solution, the Sb-based electrodes clearly display a new reduction wave at about −1.6 V which can be associated with the electrochemical reduction of $CO_2$. This behaviour is comparable with that previously observed with other Sn and Bi nanostructures [69,70,76]. It is worth noting that this contribution is not observed with the Sb rod (Fig. S6). Taken into account that the Sb NPs are dispersed on Vulcan XC-72R and subsequently air-brushed in a toray paper, it is important to demonstrate that these carbon substrates are inactive for the $CO_2$ reduction. At this respect, Fig. S8 shows the response of a blank electrode only containing these carbon substrates both in Ar and $CO_2$ saturated solutions. The results clearly indicate that these carbon materials do not significantly contribute to the $CO_2$ reduction. Taken into consideration that the $CO_2$ reduction wave with the Sb-based electrodes is observed about −1.6 V and that the electrochemical reduction of $Sb_2O_3$ to Sb takes place at much lower potentials (about −0.9 V), this points out that the active materials for $CO_2$ reduction is metallic Sb.

To investigate the surface area of the Sb/C electrodes, electrochemical capacitance measurements were performed. Figs. S9 and S10 show the results obtained. The experiments were performed in the three-electrode configuration glass cell in Ar saturated solution. The response of the Sb/C electrodes was compared with a Toray paper, a Sb rod and two electrodes only containing carbon Vulcan. The Vulcan carbon loadings were 0.63 and 1.28 mg carbon Vulcan $cm^{-2}$, which correspond with a carbon loading of 85.5 wt% of the Sb/C electrodes. It is worth recalling that the metal loading was found to be about 14.5 wt% (ICP-OES measurements). In addition, the Vulcan carbon was exposed to the same chemicals used in the synthesis, subsequently washed with acetone:water (90:10) mixtures, and finally dried in an oven at 55 °C for 12 h under vacuum conditions. In all cases, a well-defined linear behaviour is found as a function of the scan rate (Fig. S10a). As expected, the Sb/C electrodes show higher capacitance than the Sb rod and the toray paper electrode but also higher than the corresponding Vulcan-based electrodes (Fig. S10b).

### 3.4. Chronoamperometric measurements

$CO_2$ electroreduction electrolyses were carried out by chronoamperometry measurements at controlled potential in a H-type

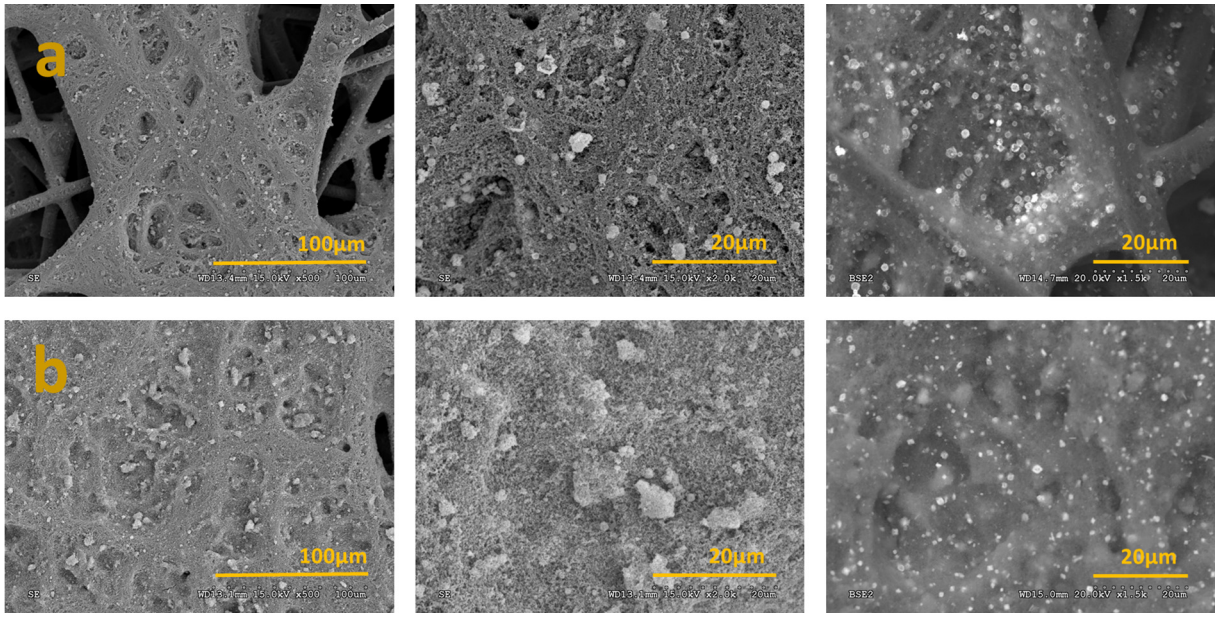


**Fig. 2.** Back-scattered electrons field emission SEM images of the Sb-based electrodes with a Sb/C loading of a) 0.75 mg $cm^{-2}$ and b) 1.50 mg $cm^{-2}$.

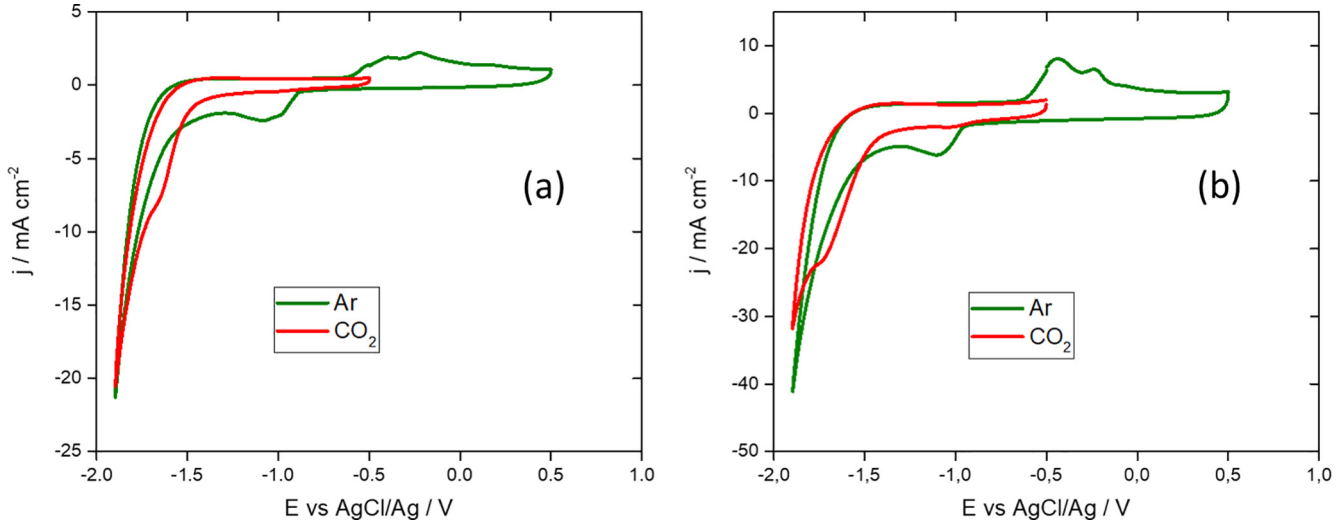


**Fig. 3.** Cyclic voltammetry response of Sb/C electrodes with (a) loading of 0.75 mg $cm^{-2}$ and (b) loading of 1.50 mg $cm^{-2}$ in Ar (green line) and $CO_2$ (red line) saturated 0.45 M $KHCO_3$ and 0.5 M KCl solution. Scan rate 50 mV $s^{-1}$.

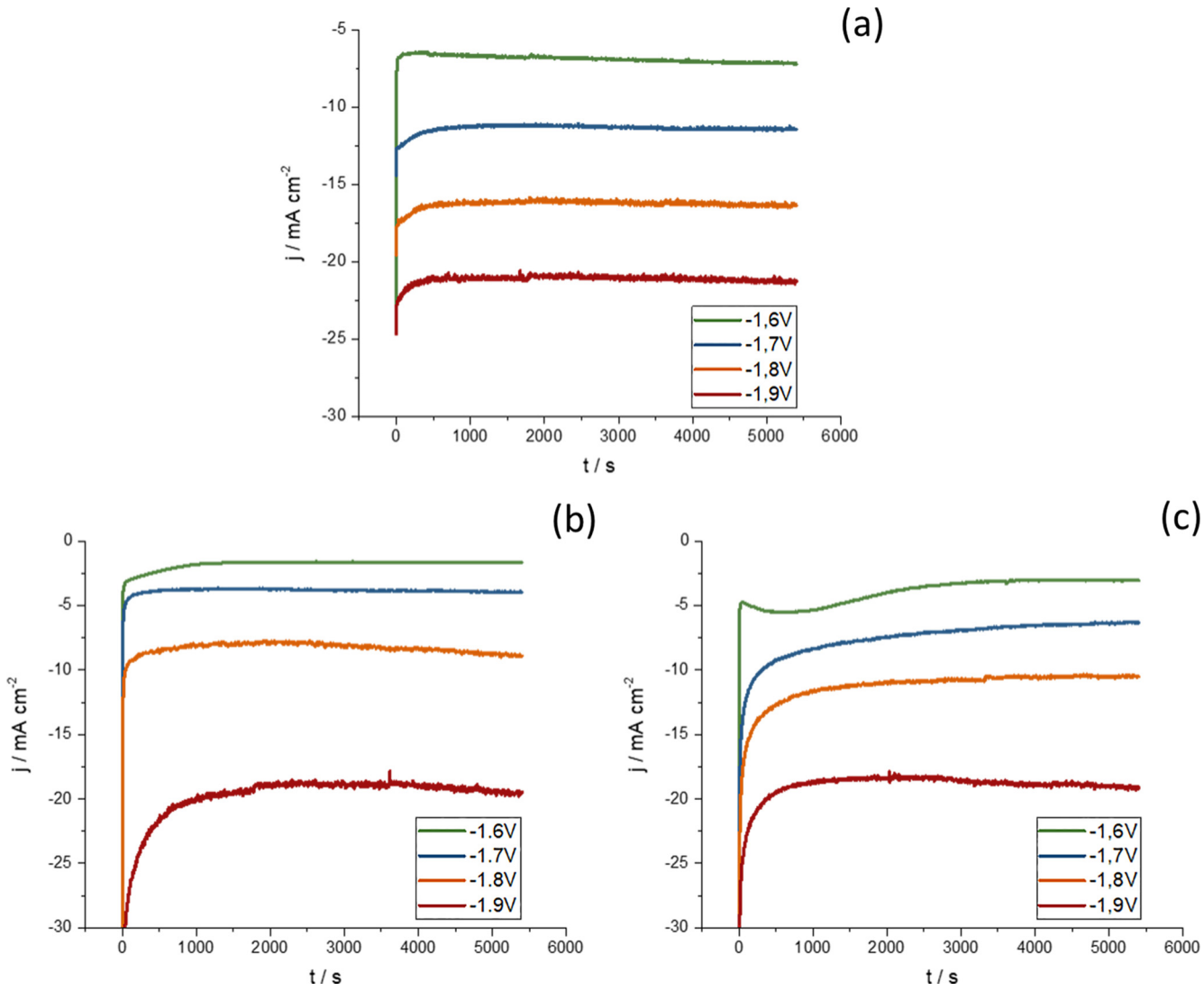


**Fig. 4.** Chronoamperometric measurements at relevant potentials for 1.5 h. a) Sb Rod, b) 0.75 mg SbC $cm^{-2}$ and c) 1.50 mg SbC $cm^{-2}$.

electrochemical cell. The faradaic efficiency and selectivity was evaluated for two different Sb/C electrodes with different catalytic loading (0.75 and 1.50 mg SbC $cm^{-2}$), and also compared with a Sb rod. The electrolyses were performed at −1.6 V, −1.7 V, −1.8 V and −1.9 V vs. AgCl/Ag in a $CO_2$-saturated 0.45 M $KHCO_3$ and 0.5 M KCl solution for 1.5 h. In these experiments, the same electrode was used for all the potentials. In these experiments, the electrode is firstly immersed into the solution at controlled potential of −1.0 V vs AgCl/Ag to completely reduce the Sb oxides. As shown in Fig. 4, the electrolysis current density remained practically constant during the entire experiments (1.5 h) at all potentials studied. Fig. 5 shows the faradaic efficiency for formate as a function of the applied potential. At the potential of −1.6 V, very low formate production was found. The faradaic efficiency values increase for more negative potential values, except for −1.9 V where it clearly drops. The cell potential ($E_{cathode-anode}$) at −1.9 V was over −8 V for both electrodes, and therefore, after 1.5 h of work at this potential, the electrodes visibly degraded due to the strong production of hydrogen bubbles. In this way, the −1.6 V and −1.9 V potentials were discarded because of the low efficiency and high degradation, respectively.

Several electrolyses were carried out at −1.7 and −1.8 V in order to evaluate the reproducibility of the faradaic efficiency values obtained. The standard deviation oscillated between 3.1 and 6.7%, demonstrating the good reproducibility of the measurements. The gaseous compounds were analysed for these experiments by gas chromatography, and only hydrogen was found, Fig. 6. Formate efficiency was very similar independently of the catalytic loadings. This suggest that only the outer layers of the electrodes are actives. In this respect, it is worth recall that increasing loading are obtained with accumulation of layer during the airbrushing of the sample on the toray paper. The highest average efficiency was achieved at −1.8 V with both electrodes, reaching values around 18–20%. These results are in good agreement with recent data using electrodeposited Sb electrodes [68]. However, previous reports such as Sb nanosheets [64] and Sb single atoms [65] display better efficiency values than our carbon-supported Sb nanoparticles. This is attributed to the unique nanostructure and properties of the nanosheets and single Sb atoms. In any case, it is worth mentioning that the present carbon supported Sb nanoparticles show remarkably higher activity compared to that obtained with the bulk Sb. In addition, the simplicity of the synthetic methodology also should be positively considered.

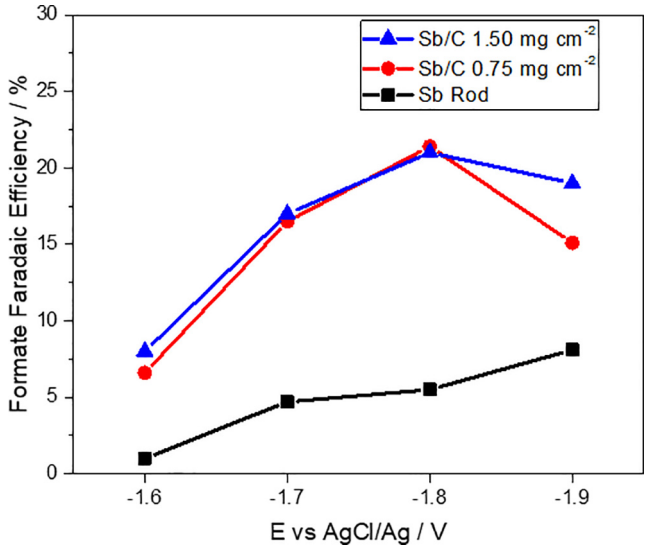


**Fig. 5.** Faradaic efficiency of formate at relevant potentials for 1.5 h of electrolysis for Sb Rod, and Sb-based electrodes (0.75 mg SbC $cm^{-2}$ and 1.50 mg SbC $cm^{-2}$).

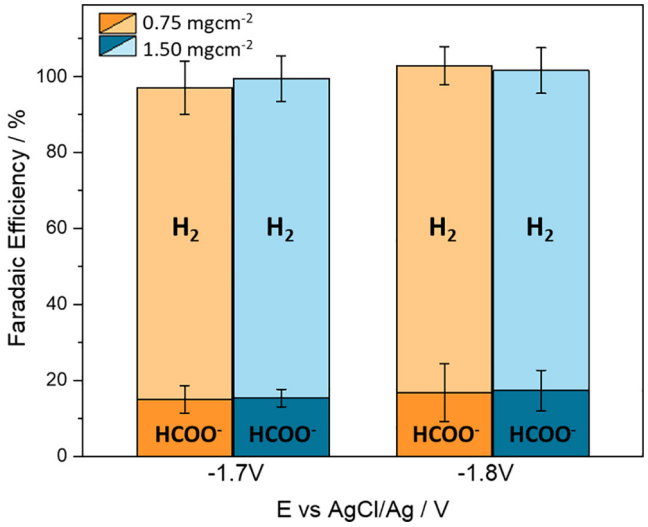


**Fig. 6.** Faradaic efficiency for formate and hydrogen productions at −1.7 and −1.8 V for different catalytic loads: 0.75 mg SbC $cm^{-2}$ and 1.50 mg SbC $cm^{-2}$. Electrolysis time: 1.5 h.

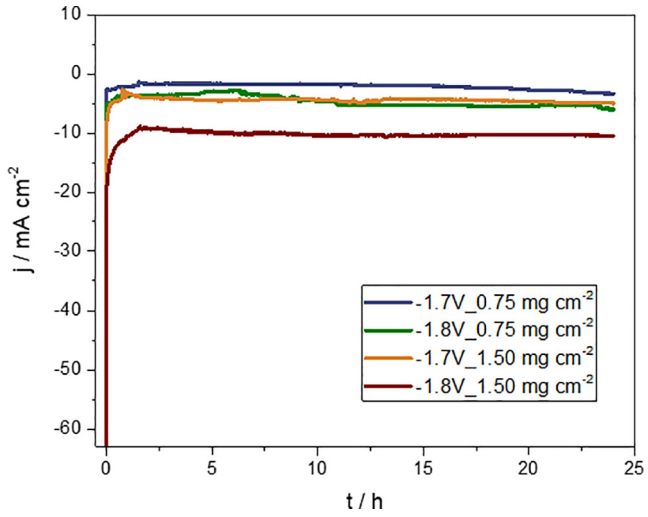


**Fig. 7.** Chronoamperometric measurements at −1.7 V and −1.8 V for 24 h.

These previous experiments seem to indicate that the stability of the Sb is better than other studied metal electrodes such as nanostructured Bi electrodes [70]. To confirm this improvement, long-term (24 h) $CO_2$ reduction experiments were carried out at − 1.7 V and −1.8 V vs. Ag/AgCl and for both electrodes (0.75 mg SbC $cm^{-2}$ and 1.50 mg SbC $cm^{-2}$) in the same H-type electrochemical cell. As shown in Fig. 7, the current remained essentially stable during the 24 h at both potentials and catalytic loadings. In addition, the formate FE also stayed stable at about 15% during 24 h for every experiment.

The results obtained indicate that these carbon-supported Sb nanoparticles, although displaying less electrocatalytic activity than other similar systems such as Sn or Bi, show an interesting stability under working conditions. In fact, as illustrated in Fig. S11, a comparison between long-term experiments of $CO_2$ electroreduction on Bi/C NPs electrode [70] and the one obtained in this work with Sb/C, clearly demonstrate the good stability of our carbon supported Sb nanoparticles under working conditions. This result is in good agreement with the good stability also reported for Sb nanosheets [64] and Sb single atoms [65] in 10–12 h experiments. This suggests that a possible incorporation of Sb on Sn and Bi can be a valuable strategy

to improve the behaviour, in terms of stability, of these Sn and Bi materials. This interesting approach has been very recently used by Lucas and Lima with electrodeposited Sn-Sb alloys for the selective and stable reduction of $CO_2$ towards formate [68]. Particularly, electrodeposited Sn9Sb1 alloy electrodes displayed improved long-term stability in comparison to pure electrodeposited Sn films. This improved stability was attributed to a lower insertion of alkali and lower formation of hydride species which minimizes the electrode disintegration. Interestingly, the Sb incorporation did not affect the FE. More work is in progress to evaluate if this strategy is also valid for nanoparticulated systems prepared using the synthetic approach here employed.

## 4. Conclusions

$Sb_2O_3$/Sb/C nanoparticles were synthesised by an easy, fast and scalable procedure at room conditions. The physicochemical characterization of these nanoparticles indicates the presence of 30 ± 10 nm $Sb_2O_3$/Sb nanoparticles which are reasonably well-dispersed on Vulcan XC-72R. The Sb-based nanoparticles display an oxidised state due to their exposure to air. The electrochemical characterization evidences that the $Sb_2O_3$ nanoparticles can be electrochemically in–situ reduced to metallic Sb and display similar voltammetric features than those shown with a Sb rod. The $Sb_2O_3$/Sb-based electrodes show a certain activity for the $CO_2$ electroreduction towards formate. In 1.5-h $CO_2$ electroreduction electrolyses, at the potentials of −1.7 V and −1.8 V vs AgCl/Cl, only hydrogen and formate were found as products. The FE towards formate was found to be about 20% independently of the metal loading (0.75 and 1.50 mg SbC $cm^{-2}$). Interestingly, the $Sb_2O_3$/Sb-based electrodes show a good stability (24-hour experiments) under working conditions. More work is in progress to take benefit of this stability and combinations of Bi and Sn (which are much better electrocatalysts for the production of formate but less stable) with Sb are being prepared with the aim of improving their stability under operation conditions. This strategy has been very recently reported with electrodeposited systems [68] but remains unexplored on nanoparticulated systems.

## CRediT authorship contribution statement

**Beatriz Ávila-Bolívar:** Investigation, Formal analysis, Visualization, Writing - original draft, Writing - review & editing. **Vicente Montiel:** Conceptualization, Funding acquisition, Supervision. **José Solla-Gullón:** Conceptualization, Funding acquisition, Supervision, Writing - review & editing.

## Declaration of Competing Interest

The authors declare that they have no known competing financial interests or personal relationships that could have appeared to influence the work reported in this paper.

## Acknowledgments

This work was supported by the MINECO, through the projects CTQ2016-76231-C2-2-R (AEI/FEDER, UE) and PID2019-108136RB-C32. Also, the invitation by the E3TECH Spanish Network of Excellence (CTQ2017-90659-REDT (MEIC/AEI)) is kindly acknowledged.

## Appendix A. Supplementary data

Supplementary data to this article can be found online at https://doi.org/10.1016/j.jelechem.2021.115440.

## References

[1] Z. Liu, S. Huang, Z. Jin, Breakpoint lead-lag analysis of the last deglacial climate change and atmospheric CO2 concentration on global and hemispheric scales, Quat. Int. 490 (2018) 50–59. https://doi.org/https://doi.org/10.1016/j.quaint.2018.05.021.
[2] O. Hoegh-Guldberg, D. Jacob, M. Taylor, T. Guillén Bolaños, M. Bindi, S. Brown, I.A. Camilloni, A. Diedhiou, R. Djalante, K. Ebi, F. Engelbrecht, J. Guiot, Y. Hijioka, S. Mehrotra, C.W. Hope, A.J. Payne, H.-O. Pörtner, S.I. Seneviratne, A. Thomas, R. Warren, G. Zhou, The human imperative of stabilizing global climate change at 1.5°C, Science 365 (2019) eaaw6974. https://doi.org/10.1126/science.aaw6974.
[3] A. Mikhaylov, N. Moiseev, K. Aleshin, T. Burkhardt, Global climate change and greenhouse effect, Entrep. Sustain. Issues. 7 (2020) 2897.
[4] J.D. Figueroa, T. Fout, S. Plasynski, H. McIlvried, R.D. Srivastava, Advances in CO2 capture technology—The U.S. Department of Energy's Carbon Sequestration Program, Int. J. Greenh. Gas Control. 2 (2008) 9–20. https://doi.org/https://doi.org/10.1016/S1750-5836(07)00094-1.
[5] M.M. Maroto-Valer, Developments and Innovation in Carbon Dioxide (CO2) Capture and Storage Technology: Carbon Dioxide (CO2) Storage and Utilisation, Elsevier, 2010.
[6] M. Aresta, A. Dibenedetto, A. Angelini, Catalysis for the valorization of exhaust carbon: from CO2 to chemicals, materials, and fuels. Technological use of CO2, Chem. Rev. 114 (3) (2014) 1709–1742, https://doi.org/10.1021/cr4002758.
[7] R.M. Cuéllar-Franca, A. Azapagic, Carbon capture, storage and utilisation technologies: A critical analysis and comparison of their life cycle environmental impacts, J. CO2 Util. 9 (2015) 82–102. https://doi.org/https://doi.org/10.1016/j.jcou.2014.12.001.
[8] K.A. Mumford, Y. Wu, K.H. Smith, G.W. Stevens, Review of solvent based carbon-dioxide capture technologies, Front. Chem. Sci. Eng. 9 (2) (2015) 125–141.
[9] T. Bruhn, H. Naims, B. Olfe-Kräutlein, Separating the debate on CO2 utilisation from carbon capture and storage, Environ. Sci. Policy. 60 (2016) 38–43.
[10] E.I. Koytsoumpa, C. Bergins, E. Kakaras, The CO2 economy: review of CO2 capture and reuse technologies, J. Supercrit. Fluids. 132 (2018) 3–16.
[11] M.Z. Jacobson, The health and climate impacts of carbon capture and direct air capture, Energy Environ. Sci. 12 (12) (2019) 3567–3574.
[12] S. Ma, P.J.A. Kenis, Electrochemical conversion of CO2 to useful chemicals: current status, remaining challenges, and future opportunities, Curr. Opin. Chem. Eng. 2 (2013) 191–199.
[13] Y. Liu, Z. Huo, D. Sun, R. Chen, Y. Chen, S. Basu, F. Hong, F. Jin, X. Wang, J. Qiao, J. Zhang, Electrochemical Reduction of Carbon Dioxide: Fundamentals and Technologies, CRC Press, Taylor and Francis Group, 2016.
[14] J. Wu, X.-D. Zhou, Catalytic conversion of CO2 to value added fuels: Current status, challenges, and future directions, Chinese J. Catal. 37 (2016) 999–1015. https://doi.org/https://doi.org/10.1016/S1872-2067(16)62455-5.
[15] Y. Li, Q. Sun, Recent advances in breaking scaling relations for effective electrochemical conversion of CO2, Adv. Energy Mater. 6 (2016) 1600463.
[16] A.S.R. Machado, M.N. da Ponte, A.S. Reis Machado, M. Nunes da Ponte, CO2 capture and electrochemical conversion, Curr. Opin. Green Sustain. Chem. 11 (2018) 86–90. https://doi.org/https://doi.org/10.1016/j.cogsc.2018.05.009.
[17] M.-Y. Lee, K.T. Park, W. Lee, H. Lim, Y. Kwon, S. Kang, Current achievements and the future direction of electrochemical CO2 reduction: a short review, Crit. Rev. Environ. Sci. Technol. 50 (8) (2020) 769–815.
[18] R. Kortlever, J. Shen, K.J.P. Schouten, F. Calle-Vallejo, M.T.M. Koper, Catalysts and reaction pathways for the electrochemical reduction of carbon dioxide, J. Phys. Chem. Lett. 6 (20) (2015) 4073–4082, https://doi.org/10.1021/acs.jpclett.5b01559.
[19] L. Zhang, Z.-J. Zhao, J. Gong, Nanostructured materials for heterogeneous electrocatalytic CO2 reduction and their related reaction mechanisms, Angew. Chemie Int. Ed. 56 (38) (2017) 11326–11353, https://doi.org/10.1002/anie.v56.3810.1002/anie.201612214.
[20] R.M. Arán-Ais, D. Gao, B. Roldan Cuenya, Structure- and electrolyte-sensitivity in CO2 electroreduction, Acc. Chem. Res. 51 (11) (2018) 2906–2917, https://doi.org/10.1021/acs.accounts.8b00360.
[21] W. Zhang, Y. Hu, L. Ma, G. Zhu, Y. Wang, X. Xue, R. Chen, S. Yang, Z. Jin, Progress and perspective of electrocatalytic CO2 reduction for renewable carbonaceous fuels and chemicals, Adv. Sci. 5 (1) (2018) 1700275, https://doi.org/10.1002/advs.201700275.
[22] W. Yang, K. Dastafkan, C. Jia, C. Zhao, Design of electrocatalysts and electrochemical cells for carbon dioxide reduction reactions, Adv. Mater. Technol. 3 (9) (2018) 1700377, https://doi.org/10.1002/admt.v3.910.1002/admt.201700377.
[23] D.-M. Feng, Y. Sun, Z.-Q. Liu, Y.-P. Zhu, T.-Y. Ma, Designing nanostructured metal-based CO2 reduction electrocatalysts, J. Nanosci. Nanotechnol. 19 (2019) 3079–3096. https://www.ingentaconnect.com/content/asp/jnn/2019/00000019/00000006/art00003.
[24] C. Long, X. Li, J. Guo, Y. Shi, S. Liu, Z. Tang, Electrochemical reduction of CO2 over heterogeneous catalysts in aqueous solution: recent progress and perspectives, Small Methods. 3 (2019) 1800369.
[25] Y. Hori, H. Wakebe, T. Tsukamoto, O. Koga, Electrocatalytic process of CO selectivity in electrochemical reduction of CO2 at metal electrodes in aqueous media, Electrochim. Acta. 39 (1994) 1833–1839. https://doi.org/https://doi.org/10.1016/0013-4686(94)85172-7.
[26] K.P. Kuhl, T. Hatsukade, E.R. Cave, D.N. Abram, J. Kibsgaard, T.F. Jaramillo, Electrocatalytic conversion of carbon dioxide to methane and methanol on

transition metal surfaces, J. Am. Chem. Soc. 136 (40) (2014) 14107–14113, https://doi.org/10.1021/ja505791r.
[27] R.J. Lim, M. Xie, M.A. Sk, J.-M. Lee, A. Fisher, X. Wang, K.H. Lim, A review on the electrochemical reduction of CO2 in fuel cells, metal electrodes and molecular catalysts, Catal. Today. 233 (2014) 169–180. https://doi.org/https://doi.org/10.1016/j.cattod.2013.11.037.
[28] Q. Lu, F. Jiao, Electrochemical CO2 reduction: electrocatalyst, reaction mechanism, and process engineering, Nano Energy 29 (2016) 439–456.
[29] D. Gao, H. Zhou, F. Cai, J. Wang, G. Wang, X. Bao, Pd-containing nanostructures for electrochemical CO2 reduction reaction, ACS Catal. 8 (2) (2018) 1510–1519, https://doi.org/10.1021/acscatal.7b03612.
[30] D. Kim, J. Resasco, Y. Yu, A.M. Asiri, P. Yang, Synergistic geometric and electronic effects for electrochemical reduction of carbon dioxide using gold–copper bimetallic nanoparticles, Nat. Commun. 5 (2014) 4948, https://doi.org/10.1038/ncomms5948.
[31] J. Monzó, Y. Malewski, R. Kortlever, F.J. Vidal-Iglesias, J. Solla-Gullón, M.T.M. Koper, P. Rodriguez, Enhanced electrocatalytic activity of Au@Cu core@shell nanoparticles towards CO2 reduction, J. Mater. Chem. A. 3 (47) (2015) 23690–23698, https://doi.org/10.1039/C5TA06804E.
[32] X. Zhao, B. Luo, R. Long, C. Wang, Y. Xiong, Composition-dependent activity of Cu–Pt alloy nanocubes for electrocatalytic CO2 reduction, J. Mater. Chem. A. 3 (8) (2015) 4134–4138, https://doi.org/10.1039/C4TA06608A.
[33] F.-Y. Zhang, T. Sheng, N. Tian, L. Liu, C. Xiao, B.-A. Lu, B.-B. Xu, Z.-Y. Zhou, S.-G. Sun, Cu overlayers on tetrahexahedral Pd nanocrystals with high-index facets for CO2 electroreduction to alcohols, Chem. Commun. 53 (57) (2017) 8085–8088, https://doi.org/10.1039/C7CC04140C.
[34] D. Kim, C. Xie, N. Becknell, Y. Yu, M. Karamad, K. Chan, E.J. Crumlin, J.K. Nørskov, P. Yang, Electrochemical activation of CO2 through atomic ordering transformations of AuCu nanoparticles, J. Am. Chem. Soc. 139 (24) (2017) 8329–8336, https://doi.org/10.1021/jacs.7b0351610.1021/jacs.7b03516.s001.
[35] C. Shan, E.T. Martin, D.G. Peters, J.M. Zaleski, Site-selective growth of AgPd nanodendrite-modified Au nanoprisms: high electrocatalytic performance for CO2 reduction, Chem. Mater. 29 (14) (2017) 6030–6043, https://doi.org/10.1021/acs.chemmater.7b0181310.1021/acs.chemmater.7b01813.s001.
[36] H. Mistry, R. Reske, Z. Zeng, Z.-J. Zhao, J. Greeley, P. Strasser, B.R. Cuenya, Exceptional size-dependent activity enhancement in the electroreduction of CO2 over Au nanoparticles, J. Am. Chem. Soc. 136 (47) (2014) 16473–16476, https://doi.org/10.1021/ja508879j.
[37] W. Zhu, R. Michalsky, Ö. Metin, H. Lv, S. Guo, C.J. Wright, X. Sun, A.A. Peterson, S. Sun, Monodisperse Au nanoparticles for selective electrocatalytic reduction of CO2 to CO, J. Am. Chem. Soc. 135 (45) (2013) 16833–16836, https://doi.org/10.1021/ja409445p.
[38] D. Gao, H. Zhou, J. Wang, S. Miao, F. Yang, G. Wang, J. Wang, X. Bao, Size-dependent electrocatalytic reduction of CO2 over Pd nanoparticles, J. Am. Chem. Soc. 137 (13) (2015) 4288–4291, https://doi.org/10.1021/jacs.5b00046.
[39] A. Loiudice, P. Lobaccaro, E.A. Kamali, T. Thao, B.H. Huang, J.W. Ager, R. Buonsanti, Tailoring copper nanocrystals towards C2 products in electrochemical CO2 reduction, Angew. Chemie Int. Ed. 55 (19) (2016) 5789–5792, https://doi.org/10.1002/anie.201601582.
[40] K.J.P. Schouten, E. Pérez Gallent, M.T.M. Koper, The influence of pH on the reduction of CO and CO2 to hydrocarbons on copper electrodes, J. Electroanal. Chem. 716 (2014) 53–57. https://doi.org/https://doi.org/10.1016/j.jelechem.2013.08.033.
[41] A.S. Varela, M. Kroschel, T. Reier, P. Strasser, Controlling the selectivity of CO2 electroreduction on copper: the effect of the electrolyte concentration and the importance of the local pH, Catal. Today. 260 (2016) 8–13, https://doi.org/10.1016/j.cattod.2015.06.009.
[42] X. Liu, P. Schlexer, J. Xiao, Y. Ji, L. Wang, R.B. Sandberg, M. Tang, K.S. Brown, H. Peng, S. Ringe, pH effects on the electrochemical reduction of CO2 towards C2 products on stepped copper, Nat. Commun. 10 (2019) 1–10.
[43] S. Verma, X. Lu, S. Ma, R.I. Masel, P.J.A. Kenis, The effect of electrolyte composition on the electroreduction of CO2 to CO on Ag based gas diffusion electrodes, Phys. Chem. Chem. Phys. 18 (10) (2016) 7075–7084, https://doi.org/10.1039/C5CP05665A.
[44] A.S. Varela, W. Ju, T. Reier, P. Strasser, Tuning the catalytic activity and selectivity of Cu for CO2 electroreduction in the presence of halides, ACS Catal. 6 (4) (2016) 2136–2144, https://doi.org/10.1021/acscatal.5b0255010.1021/acscatal.5b02550.s001.
[45] J. Medina-Ramos, S.S. Lee, T.T. Fister, A.A. Hubaud, R.L. Sacci, D.R. Mullins, J.L. DiMeglio, R.C. Pupillo, S.M. Velardo, D.A. Lutterman, J. Rosenthal, P. Fenter, Structural dynamics and evolution of bismuth electrodes during electrochemical reduction of CO2 in imidazolium-based ionic liquid solutions, ACS Catal. 7 (2017) 7285–7295. https://doi.org/10.1021/acscatal.7b01370.
[46] J. Herranz, J. Durst, E. Fabbri, A. Patru, X. Cheng, A.A. Permyakova, T.J. Schmidt, Interfacial effects on the catalysis of the hydrogen evolution, oxygen evolution and CO2-reduction reactions for (co-)electrolyzer development, Nano Energy. 29 (2016) 4–28. https://doi.org/https://doi.org/10.1016/j.nanoen.2016.01.027.
[47] K.-J. Jeong, C.M. Miesse, J.-H. Choi, J. Lee, J. Han, S.P. Yoon, S.W. Nam, T.-H. Lim, T. G. Lee, Fuel crossover in direct formic acid fuel cells, J. Power Sources. 168 (2007) 119–125. https://doi.org/https://doi.org/10.1016/j.jpowsour.2007.02.062.
[48] N.V. Rees, R.G. Compton, Sustainable energy: a review of formic acid electrochemical fuel cells, J. Solid State Electrochem. 15 (10) (2011) 2095–2100, https://doi.org/10.1007/s10008-011-1398-4.
[49] M. Pérez-Fortes, J.C. Schöneberger, A. Boulamanti, G. Harrison, E. Tzimas, Formic acid synthesis using CO2 as raw material: techno-economic and environmental evaluation and market potential, Int. J. Hydrogen Energy. 41 (2016) 16444–16462, https://doi.org/10.1016/j.ijhydene.2016.05.199.
[50] A. Álvarez, A. Bansode, A. Urakawa, A.V. Bavykina, T.A. Wezendonk, M. Makkee, J. Gascon, F. Kapteijn, Challenges in the greener production of formates/formic acid, methanol, and DME by heterogeneously catalyzed CO2 hydrogenation processes, Chem. Rev. 117 (14) (2017) 9804–9838, https://doi.org/10.1021/acs.chemrev.6b00816.
[51] B.C. Ong, S.K. Kamarudin, S. Basri, Direct liquid fuel cells: a review, Int. J. Hydrogen Energy. 42 (2017) 10142–10157, https://doi.org/10.1016/j.ijhydene.2017.01.117.
[52] M. Rumayor, A. Dominguez-Ramos, A. Irabien, Formic acid manufacture: carbon dioxide utilization alternatives, Appl. Sci. 8 (2018) 914, https://doi.org/10.3390/app8060914.
[53] M. Czaun, J. Kothandaraman, A. Goeppert, B. Yang, S. Greenberg, R.B. May, G.A. Olah, G.K.S. Prakash, Iridium-Catalyzed Continuous Hydrogen Generation from Formic Acid and Its Subsequent Utilization in a Fuel Cell: Toward a Carbon Neutral Chemical Energy Storage, ACS Catal. 6 (11) (2016) 7475–7484, https://doi.org/10.1021/acscatal.6b0160510.1021/acscatal.6b01605.s001.
[54] A.K. Singh, S. Singh, A. Kumar, Hydrogen energy future with formic acid: a renewable chemical hydrogen storage system, Catal. Sci. Technol. 6 (1) (2016) 12–40, https://doi.org/10.1039/C5CY01276G.
[55] J. Wu, F.G. Risalvato, F.-S. Ke, P.J. Pellechia, X.-D. Zhou, Electrochemical reduction of carbon dioxide I. Effects of the electrolyte on the selectivity and activity with Sn electrode, J. Electrochem. Soc. 159 (7) (2012) F353–F359, https://doi.org/10.1149/2.049207jes.
[56] A. Del Castillo, M. Alvarez-Guerra, A. Irabien, Continuous electroreduction of CO2 to formate using Sn gas diffusion electrodes, AIChE J. 60 (10) (2014) 3557–3564, https://doi.org/10.1002/aic.14544.
[57] D.H. Won, C.H. Choi, J. Chung, M.W. Chung, E.-H. Kim, S.I. Woo, Rational design of a hierarchical tin dendrite electrode for efficient electrochemical reduction of CO2, ChemSusChem 8 (18) (2015) 3092–3098, https://doi.org/10.1002/cssc.201500694.
[58] H. Zhong, Y. Qiu, T. Zhang, X. Li, H. Zhang, X. Chen, Bismuth nanodendrites as a high performance electrocatalyst for selective conversion of CO2 to formate, J. Mater. Chem. A. 4 (36) (2016) 13746–13753, https://doi.org/10.1039/C6TA06202D.
[59] C. Zhao, J. Wang, Electrochemical reduction of CO2 to formate in aqueous solution using electro-deposited Sn catalysts, Chem. Eng. J. 293 (2016) 161–170, https://doi.org/10.1016/j.cej.2016.02.084.
[60] S. Kim, W.J. Dong, S. Gim, W. Sohn, J.Y. Park, C.J. Yoo, H.W. Jang, J.-L. Lee, Shape-controlled bismuth nanoflakes as highly selective catalysts for electrochemical carbon dioxide reduction to formate, Nano Energy 39 (2017) 44–52, https://doi.org/10.1016/j.nanoen.2017.05.065.
[61] X. Zhang, T. Lei, Y. Liu, J. Qiao, Enhancing CO2 electrolysis To formate on facilely synthesized Bi catalysts at low overpotential, Appl. Catal. B Environ. 218 (2017) 46–50, https://doi.org/10.1016/j.apcatb.2017.06.032.
[62] J. Medina-Ramos, R.C. Pupillo, T.P. Keane, J.L. DiMeglio, J. Rosenthal, Efficient conversion of CO2 to CO using tin and other inexpensive and easily prepared post-transition metal catalysts, J. Am. Chem. Soc. 137 (15) (2015) 5021–5027, https://doi.org/10.1021/ja5121088.
[63] M. Jia, S. Hong, T.-S. Wu, X. Li, Y.-L. Soo, Z. Sun, Single Sb sites for efficient electrochemical CO2 reduction, Chem. Commun. 55 (80) (2019) 12024–12027, https://doi.org/10.1039/C9CC06178A.
[64] F. Li, M. Xue, J. Li, X. Ma, L. Chen, X. Zhang, D.R. MacFarlane, J. Zhang, Unlocking the electrocatalytic activity of antimony for CO2 reduction by two-dimensional engineering of the bulk material, Angew. Chemie Int. Ed. 56 (2017) 14718–14722. https://doi.org/https://doi.org/10.1002/anie.201710038.
[65] Z. Jiang, T. Wang, J. Pei, H. Shang, D. Zhou, H. Li, J. Dong, Y. Wang, R. Cao, Z. Zhuang, W. Chen, D. Wang, J. Zhang, Y. Li, Discovery of main group single Sb–N4 active sites for CO2 electroreduction to formate with high efficiency, Energy Environ. Sci. 13 (9) (2020) 2856–2863, https://doi.org/10.1039/D0EE01486A.
[66] S. Rasul, A. Pugnant, E. Yu, Electrochemical reduction of CO2 at multi-metallic interfaces, ECS Trans. 85 (10) (2018) 57–66, https://doi.org/10.1149/08510.0057ecst.
[67] S. Rasul, A. Pugnant, H. Xiang, J.-M. Fontmorin, E.H. Yu, Low cost and efficient alloy electrocatalysts for CO2 reduction to formate, J. CO2 Util. 32 (2019) 1–10. https://doi.org/https://doi.org/10.1016/j.jcou.2019.03.016.
[68] F.W.S. Lucas, F.H.B. Lima, Electrodeposited tin-antimony alloys as novel electrocatalysts for selective and stable carbon dioxide reduction to formate, ChemElectroChem. 7 (2020) 3733–3742. https://doi.org/https://doi.org/10.1002/celc.202000769.
[69] A. Del Castillo, M. Alvarez-Guerra, J. Solla-Gullón, A. Sáez, V. Montiel, A. Irabien, Sn nanoparticles on gas diffusion electrodes: Synthesis, characterization and use for continuous CO2 electroreduction to formate, J. CO2 Util. 18 (2017) 222–228. https://doi.org/https://doi.org/10.1016/j.jcou.2017.01.021.
[70] B. Ávila-Bolívar, L. García-Cruz, V. Montiel, J. Solla-Gullón, Electrochemical reduction of CO2 to formate on easily prepared carbon-supported Bi nanoparticles, Molecules 24 (11) (2019) 2032, https://doi.org/10.3390/molecules24112032.
[71] I. Sanjuán, L. García-Cruz, J. Solla-Gullón, E. Expósito, V. Montiel, Bi–Sn nanoparticles for electrochemical denitrification: activity and selectivity towards N2 formation, Electrochim. Acta. 340 (2020), https://doi.org/10.1016/j.electacta.2020.135914 135914.
[72] R.L. Zhang, S.Z. Tang, Preparation of ultrafine cubic Sb2O3 crystals under ultrasonic, Ultrason. Sonochem. 22 (2015) 155–159. https://doi.org/https://doi.org/10.1016/j.ultsonch.2014.06.021.

[73] F. Garbassi, XPS and AES study of antimony oxides, Surf. Interface Anal. 2 (5) (1980) 165–169.
[74] D.J. Morgan, Metallic antimony (Sb) by XPS, Surf. Sci. Spectra. 24 (2) (2017) 024004, https://doi.org/10.1116/1.4994636.
[75] E. Nolot, C. Sabbione, W. Pessoa, L. Prazakova, G. Navarro, Germanium, antimony, tellurium, their binary and ternary alloys and the impact of nitrogen: An X-ray photoelectron study, Appl. Surf. Sci. 536 (2021), https://doi.org/10.1016/j.apsusc.2020.147703 147703.
[76] G. Díaz-Sainz, M. Alvarez-Guerra, B. Ávila-Bolívar, J. Solla-Gullón, V. Montiel, A. Irabien, Improving trade-offs in the figures of merit of gas-phase single-pass continuous CO2 electrocatalytic reduction to formate, Chem. Eng. J. 405 (2021), https://doi.org/10.1016/j.cej.2020.126965 126965.